Received 5 July 2025; revised 8 August 2025; accepted 12 August 2025. Date of publication 15 August 2025; date of current version 4 September 2025. The review of this article was arranged by Associate Editor Lefei Ge.

Digital Object Identifier 10.1109/OJIES.2025.3599390

Time-Efficient and Practical Design Method for Skewed PMSMs: Integrating Numerical Calculations With Limited 3-D-FEA

REN TSUNATA (Member, IEEE), YU ICHIMURA, MASATSUGU TAKEMOTO (Member, IEEE), AND JUN IMAI (Member, IEEE)

Graduate School of Environmental, Life, Natural Science and Technology, Okayama University, Okayama 700-8530, Japan CORRESPONDING AUTHOR: REN TSUNATA (e-mail: tsunata@okayama-u.ac.jp).

ABSTRACT This article proposes a time-efficient and practical design method for determining appropriate skew structures for permanent magnet synchronous motors (PMSMs). Various PMSMs use skew to suppress torque ripple, but 3-D finite element analysis (3-D-FEA) is required in order to accurately determine an appropriate structure for skewed PMSMs, resulting in a long analysis time. Therefore, this article constructs a hybrid analysis method that combines numerical calculations and minimal 3-D-FEA. The aim of this method is to be practical and easy to use, even for novice designers, and to accurately and quickly design skewed PMSMs. In this article, the effectiveness of the proposed method is clarified through several case studies, and then, a skewed PMSM designed using the proposed method is verified experimentally. It is also revealed that suppression of voltage harmonics contributes to improving the performance of PMSMs in experiments.

INDEX TERMS Design method, efficiency, field weakening control, interior permanent magnet synchronous motor (IPMSM), PMSMs, skew, torque ripple, voltage harmonics.

NOMENCLATURE

 N_p Number of poles. N_s Number of slots.

M Number of steps in step skew.

 θ_{cog} Angle of one cycle of cogging torque.

 $\theta_{
m skew_theo}$ Theoretical skew angle. $\theta_{
m skew_step}$ Skew angle for each step.

 θ_{skew} Total skew angle. β Current phase angle.

I. INTRODUCTION

A. RESEARCH OBJECTIVES

In recent years, permanent magnet synchronous motors (PMSMs) have been used in various applications because of their high performance [1], [2]. In some applications, it is necessary to suppress torque ripple and cogging torque and to reduce the harmonics of the induced voltage [3]. To meet such requirements, skew is frequently adopted in PMSMs [4], [5]. This technology is well established, and PMSMs using skew are comprehensively discussed in [6], including

practical examples and the advantages, and challenges of each structure. Although skewed PMSMs can be broadly classified into various structures, this article focuses on rotor step skew because it is widely used.

Clarifying the characteristics of skewed PMSMs requires 3-D finite element analysis (3-D-FEA), the development of which is time-consuming. For this reason, many methods have been proposed for the rapid design of skewed PMSMs. Furthermore, the increasing use of skewed PMSMs results in many situations where novice designers must determine appropriate skew parameters, but the design methods considered to date require complex theories, formulas, or analytical models. Therefore, this article proposes a practical design method that can be used for skewed PMSMs accurately and rapidly, but that is simple and easy to use even for novice designers.

Moreover, whereas most of previous investigations considered skew for only the purpose of suppressing cogging torque and torque ripple, it is known that induced voltage harmonics increase during the field-weakening control of PMSMs. However, there has been little investigation of the effect of these harmonics on the operating characteristics of PMSMs.

TABLE 1. Summary of Conventional Design Methods for Skewed PMSMs

Method	Reference No.	
Flux-MMF diagram	[8]	
Equivalent magnetic circuit	[9],[10],[18]	
Analytical calculation	[11], [12], [13], [14], [15]	
Subdomain model	[16], [17], [18]	
Multi slice model	[19], [20], [21], [22], [23],	
	[24], [25], [26], [27]	
Genetic algorithm	[28], [29]	
Other proposed methods	[30], [31], [32], [33]	

This article therefore clarifies the operating characteristics experimentally when the voltage harmonics are reduced by using a skewed PMSM. Also, skew is shown to be effective in improving the efficiency of PMSMs during the field-weakening control.

In summary, the main objectives of this study are as follows.

- To propose a time-efficient, practical, and simple design method for skewed PMSMs.
- 2) To evaluate the effect of voltage harmonics on improving the operating characteristics of a prototype machine.

B. CONVENTIONAL DESIGN METHODS

Skewing techniques suppress torque fluctuations for each angle by generally shifting the rotor or stator of a PMSM in the circumferential direction. However, when skew is adopted, 3-D-FEA is required to clarify the characteristics of the PMSMs [7]. As a result, a long analysis time is needed to search for an appropriate skew structure. Therefore, many research groups have investigated ways to shorten the development and analysis time of skewed PMSMs.

Table 1 summarizes the conventional analysis methods for skewed PMSMs. The early calculation methods used flux-magnetomotive force (MMF) and equivalent magnetic circuits (EMCs) [8], [9], [10]; EMCs were often used to design unskewed PMSMs but their use expanded to consider skew as well. However, with these methods, it is difficult to consider fringing flux and the effects of magnetic saturation are often ignored, resulting in large errors in the design of skewed PMSMs.

Various methods were subsequently developed to calculate electromagnetic characteristics analytically, for example, by using the Fourier series method [11]. For example, calculation methods based on the transfer relation and energy method [12], [13], [14] were considered. In addition, a calculation has also been proposed that considers local inhomogeneous saturation by combining the vector superposition method and the virtual magnetic field of the rotor [15]. However, these analytical calculations require the construction of complex mathematical models, and compared with FEA, the errors

are particularly large in the magnetic saturation region. In addition, a calculation method using a subdomain model was proposed as a derivative of the analytical calculation [16], [17]. A hybrid method combining a method using a subdomain model with EMC was also considered, achieving a short analysis time [18].

The most commonly used method for shortening the analysis time for skewed PMSMs is the multislice method; the PMSM is divided into several 2-D cross sections, and the skew is considered by combining it with analytical calculation or FEA [19]. Various multislice methods have been proposed, including a method using a lookup table [20], a method considering not only the skew but also rotor torsion [21], and a method considering magnetic saturation and interference between the d-axis and q-axis [22]. Recently, the multislice method has also been applied to noise-vibrationharshness analysis [23]. In particular, the authors in [24] and [25] showed that the results are relatively consistent with those of 3-D-FEA. However, Lazari et al. [26] found that the error in 2-D-FEA increases when leakage flux occurs between each step of the step skew. Finally, Lazari et al. [26] concluded that the multislice method cannot consider 3-D effects. Accordingly, Klausnitzer and Moeckel [27] proposed a method to improve accuracy by analyzing the end effect using 3-D-FEA and incorporating it into the multislice method. However, concerns remain because it still cannot consider axial magnetic flux leakage between each step of the step skew.

In addition, the design of skewed PMSMs using a genetic algorithm has also been proposed and its effectiveness has been demonstrated [28], [29]. However, there are concerns that genetic algorithms require long analysis time and that the solution will also be affected by the choice of initial conditions. Other analysis methods have also been proposed, such as a method that detects all peak values using the contour line concept coupled with Kriging [30] and a method that uses the novel coefficient modeling [31], but they require complex modeling and the combination of multiple methods, which would be difficult for novice designers.

In addition, Won et al. [32] proposed a method to shorten the design period of skewed PMSMs by combining a large amount of 2-D-FEA-based data with a small amount of 3-D-FEA using a surrogate model. However, this method requires a large amount of 2-D-FEA, and the accuracy of the results may be affected by the number and accuracy of the training data. Furthermore, Ocak and Aydin [33] proposed a design method for skewed PMSMs using semi-FEA, considering optimization of the axial length of each step. However, because 2-D-FEA is used, 3-D effects are not considered. As a result, there are concerns about large errors due to axial leakage flux between steps, especially in interior PMSMs (IPMSMs) [6]. Moreover, although much research has focused on cogging torque in skewed PMSMs, high efficiency is also important, and Koo et al. [34] stated that 3-D-FEA is essential when considering the eddy current loss in the magnets of skewed PMSMs.

Considering the above, the following main problems can be identified in the conventional analysis methods for skewed PMSMs.

- 1) Many methods do not consider 3-D effects, and errors are large because of end effects and axial flux leakage between steps (especially in IPMSMs).
- The mathematical model and formula construction are very complicated, making the methods difficult for novice designers to use.
- 3) In the method that uses 3-D-FEA for correction, correction is not generally performed during the design process, so errors may occur depending on the correction method for the initial conditions.

C. CONTRIBUTION OF THIS PAPER

The design method proposed in this article combines simple numerical calculations with a minimal amount of 3-D-FEA. Under a constraint on the number of steps *M* determined by the designer, an appropriate skew angle is calculated numerically, and errors are corrected during the calculation using a minimal amount of 3-D-FEA. Because the proposed design method can be applied to any rotor structure and operating conditions, it is highly versatile and can design an appropriate skewed model rapidly with high accuracy.

In addition, a method of correcting errors using 3-D-FEA during simple numerical analysis has not yet been considered. Although the total analysis time could increase in comparison with some of the conventional methods in Table 1, the proposed method is simple, with few errors and straightforward calculations that can be realized using magnetic field analysis software and Excel, etc. As a result, even novice designers can realize a high-performance skewed PMSM with high accuracy because complex models or theories are not required. In addition, because the processing power of computers used for magnetic field analysis has improved dramatically in recent years, the authors expect that many more research groups will be able to perform 3-D-FEA in the future, and the proposed method is a suitable candidate as a very practical method in such cases.

Part of the proposed design method was previously reported in [35], but with no discussion of accuracy, case studies, or robustness. Furthermore, the present article newly includes experimental verification using prototype IPMSMs that have unskewed and skewed rotors. In addition, most previous studies on skewed PMSMs focused on suppressing torque ripple and cogging torque. However, the aims of this article are to design a skewed PMSM to suppress voltage harmonics and to clarify the effects of voltage harmonics on the operating characteristics in experiments.

The rest of this article is organized as follows. Section II presents the design of an optimal skew model using a parametric study with 3-D-FEA and explains the error between the theoretical skew angle and the actual optimal skew angle. This section also explains the harmonics of the induced voltage during the field-weakening control, and describes the need for an appropriate design method for skewed PMSMs.

Section III details the proposed method using a flowchart and 3-D models of the design process, and also verifies the effectiveness of a skewed PMSM designed using the proposed method. Section IV verifies the accuracy and robustness of the proposed design method through multiple case studies with different constraints. Section V evaluates the accuracy of the proposed design method from multiple viewpoints by experimental verification using a prototype skewed PMSM designed using the proposed method. In addition, the effect of voltage harmonics on operating characteristics is verified by comparison of prototype unskewed and skewed PMSMs. Section VI concludes this article.

II. DESIGN ISSUES WITH SKEWED PMSMS

A. THEORETICAL SKEW ANGLE

In skewed PMSMs, the theoretical skew angle $\theta_{\text{skew_theo}}$ at which the cogging torque is minimum can be calculated using the following equation [14]:

$$\theta_{\text{skew_theo}} = \theta_{\text{cog}} = \frac{360^{\circ} \times \text{GCD}(N_p, N_s)}{N_p N_s}$$
 (1)

where N_p and N_s are the number of poles and the number of slots in the PMSM, respectively, and $GCD(N_p, N_s)$ is the greatest common divisor of N_p and N_s . The theoretical skew angle determined only by the number of poles and slots is the same as the period $\theta_{\rm cog}$ of the cogging torque. In addition, in the step skew, the skew angle that minimizes the cogging torque when the number of steps M is taken into consideration is given by

$$\theta_{\text{skew}} = \frac{M-1}{M} \times \frac{360^{\circ}}{\text{LCM}(N_p, N_s)}$$
 (2)

where $LCM(N_p, N_s)$ is the least common multiple of N_p and N_s . In addition, the skew angle for each step, $\theta_{\text{skew_step}}$, is calculated as follows [16]:

$$\theta_{\text{skew_step}} = \frac{\theta_{\text{skew}}}{M - 1} \tag{3}$$

and thus, the optimal skew angle can be theoretically calculated

B. OPTIMAL SKEW ANGLE DETERMINED BY PARAMETRIC STUDY

This subsection evaluates the error between the skew angle calculated by (2) and the optimal skew angle determined by a parametric study using 3-D-FEA. The motor considered is an IPMSM, which is often used in applications, such as traction motors that require suppression of torque ripple [36], [37]. Fig. 1 shows the investigated model, in which the stator has a distributed winding structure. Table 2 shows the main parameters of the investigated model, where the number of poles N_p is 6 and the number of slots N_s is 36.

Fig. 2 shows the total harmonic distortion (THD) of the induced voltage for the investigated model in Fig. 1 when the maximum current of 10 Arms is applied with the current phase angle $\beta = 40^{\circ}$. The skew angle that minimizes

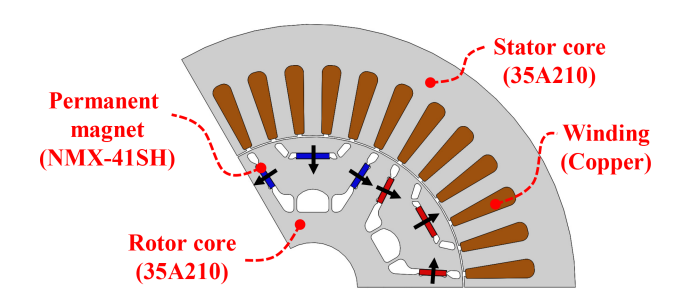


FIGURE 1. Investigated model using IPM structure.

TABLE 2. Basic Parameters of Investigated Model

Item	Value	
Number of poles/slots	6p/36 s	
Outer diameter of stator	147.2 mm	
Outer diameter of rotor	84.2 mm	
Stack length	75.6 mm	
Air gap length	0.4 mm	
Phase resistance per coil	0.143 mm	
Maximum speed	7200 r/min	
DC bus voltage	141 V	
Maximum current	10 Arms	

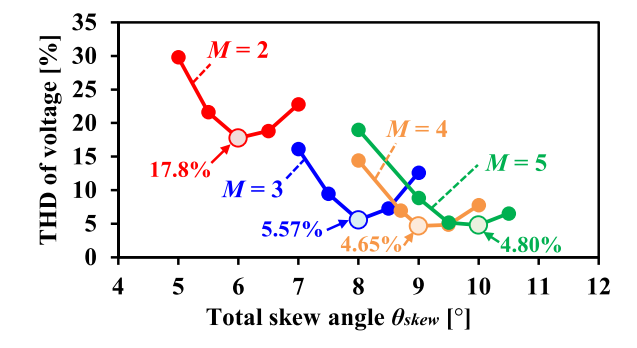


FIGURE 2. Determination of total skew angle $\theta_{\rm skew}$ that minimizes THD in IPMSM using conventional skew under conditions with 10 Arms and $\beta=40^{\circ}$.

the THD is determined by a parametric study for each case involving a different number of steps M. Increasing M tends to result in smaller THD. In addition, as M increases, so too does the skew angle $\theta_{\rm skew}$ at which the THD is minimized. However, for sufficiently large M, the resulting decrease in THD becomes smaller. Fig. 3 shows models of the skew angle at which the THD is minimized for each number of steps M in Fig. 2.

Fig. 4 compares the theoretical skew angle $\theta_{\rm skew}$ for each number of steps M obtained by (2) and the optimal skew angle $\theta_{\rm skew}$ at which the THD of the IPMSM is minimized by 3-D-FEA. The 3-D-FEA conditions are 7200 r/min and 10 Arms with a current phase angle $\beta=40^\circ$ which gives the maximum torque. There is a large error between the theoretical skew angle in (2) and the optimal angle obtained by 3-D-FEA. This means that the appropriate skew angle varies greatly

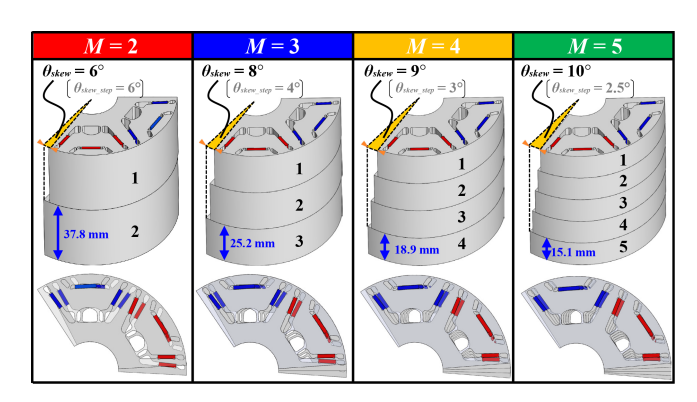


FIGURE 3. Models using conventional step skew that minimize THD of voltage for each number of steps M.

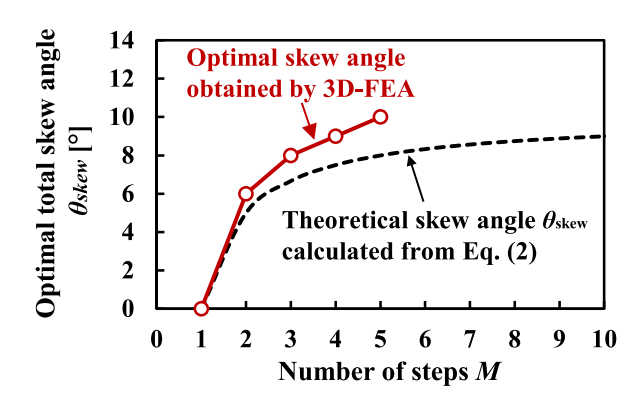


FIGURE 4. Comparison between theoretically calculated skew angle and optimal skew angle obtained by parametric study with 3-D-FEA at 10 Arms and $\beta=40^\circ$.

depending on the waveform of the induced voltage because the THD is calculated using the sum of all harmonic components. On the other hand, it is known that the cogging torque is in good agreement between the theoretical skew angle and the actual skew angle.

The above shows that the THD of the induced voltage, in particular, is not necessarily minimized at the theoretically determined skew angle because the frequency component and magnitude change depending on various parameters, such as the armature current. Therefore, a design method is required that can quickly and accurately determine the skew angle $\theta_{\rm skew}$ that minimizes the THD of the induced voltage depending on the operating conditions and structure.

C. SLOT HARMONICS

In general, the induced voltage waveform includes the slot harmonics that vary with the armature current. Here, the impact of the armature current on the slot harmonics is evaluated and described. In traction motors, field-weakening control is used during high-speed operation [38]. Although the current phase angle β of the input current increases in this case, there is a possibility that the slot harmonics may become superimposed on the induced voltage [39]. The magnetic flux densities of the unskewed IPMSM are simulated and compared by

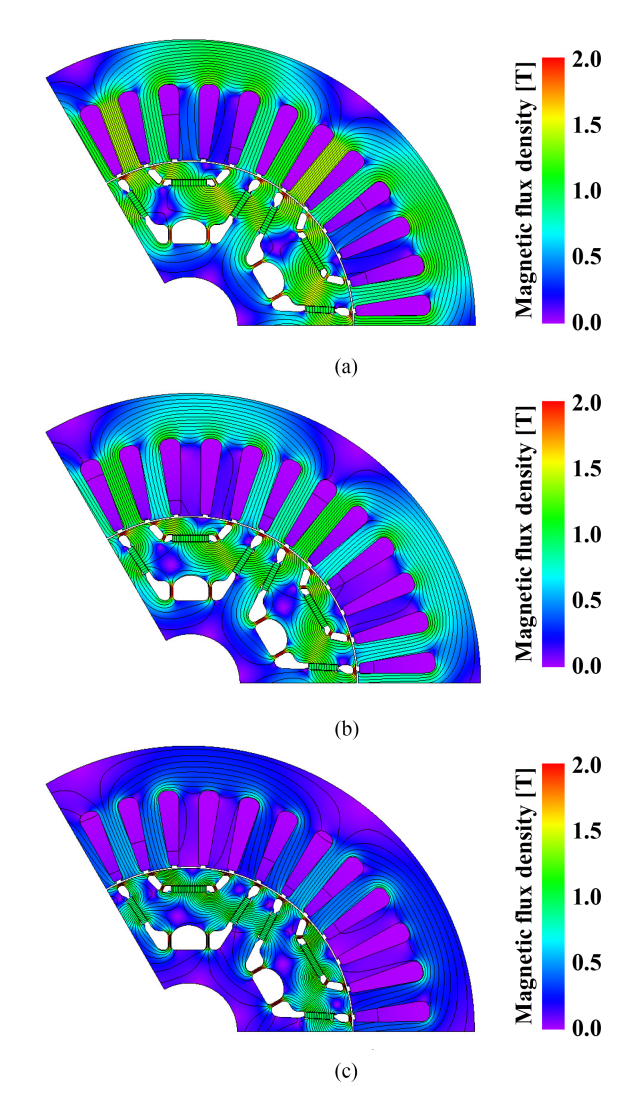


FIGURE 5. Magnetic flux density distributions of unskewed IPMSM in high-speed area at 7200 r/min and 10 Arms. (a) $\beta=0^{\circ}$. (b) $\beta=40^{\circ}$. (c) $\beta=70^{\circ}$.

2-D-FEA in Fig. 5. They are evaluated at the rated current (10 Arms) with different current phase angle at a maximum speed of 7200 r/min. Fig. 5(a) shows the case where the current phase angle is $\beta = 0^{\circ}$. As a result, only the q-axis current is applied, and this is the condition under which the magnet torque is largest. In general, the amount of magnetic flux in electric machines is the largest in such a case. Consequently, the magnetic flux densities in the stator teeth and back yoke are high, as indicated in Fig. 5(a). In contrast, as the current phase angle β is changed to 70°, the field-weakening control area is applied. Resultantly, the overall magnetic flux density decreases in the investigated IPMSM, as shown in Fig. 5(c), because the negative d-axis current increases because of the field-weakening control.

Fig. 6 compares the induced voltages and their histograms in the unskewed IPMSM. When the current phase angle β is 0° , as shown in Fig. 6(a), the fundamental voltage is high because the amount of magnetic flux is large, as described

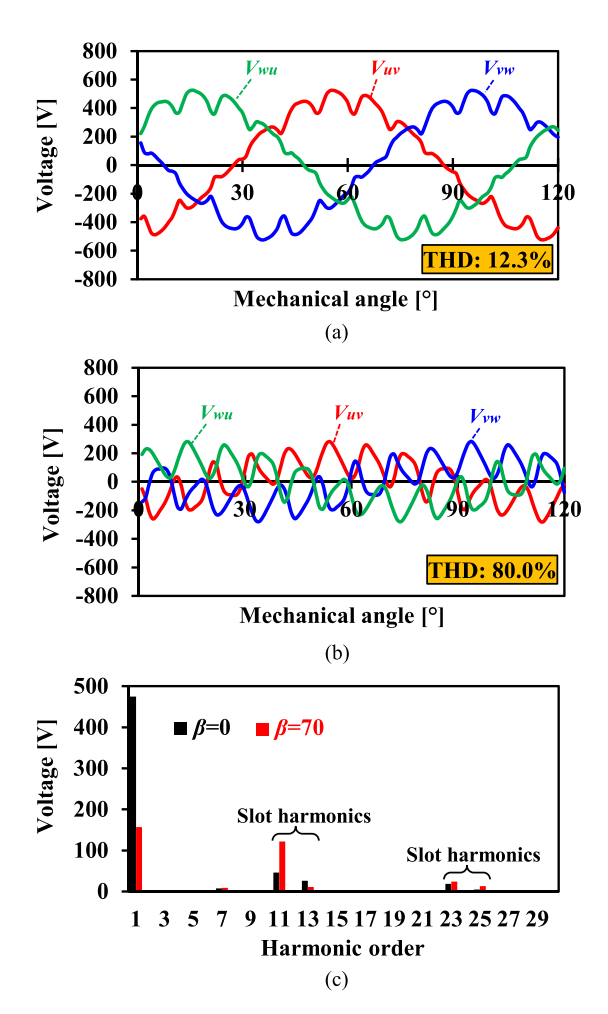


FIGURE 6. Voltage waveforms of unskewed IPMSM in high-speed area at 7200 r/min and 10 Arms. (a) $\beta = 0^{\circ}$. (b) $\beta = 70^{\circ}$. (c) Histogram.

in Fig. 5(a). The induced voltage includes small harmonics corresponding to the slotting effect. In contrast, when the current phase angle is changed to $\beta=70^\circ$, the fundamental voltage is much lower than in the case with $\beta=0^\circ$, as shown in Fig. 6(b), because of the field-weakening control. Both voltage waveforms are compared in Fig. 6(c). The fundamental voltage is reduced by the field-weakening control with the large current phase angle β of 70° . In contrast, the 11th voltage harmonic (part of the slot harmonics) increases, becoming almost the same as the fundamental voltage at $\beta=70^\circ$. When the current phase angles β is 0° and 70° , the THDs of the induced voltage is 12.3% and 80.0%, respectively. In other words, the THD of the induced voltage is increased by the field-weakening control with large current phase angle.

Thus, even when the THD of the induced voltage is reduced by skew, the appropriate skew angle may differ because the breakdown of the harmonic components of the voltage changes considerably depending on the input current conditions. In addition, the slot harmonics might affect the operating characteristics of IPMSMs in actual machines, and so this is investigated in this article using prototypes with and without the skew.

III. PROPOSED DESIGN METHOD FOR SKEWED PMSM

A. PROPOSED DESIGN METHOD

In general, evaluating the properties of skewed PMSMs requires 3-D-FEA, which is time-consuming. Therefore, this article proposes a useful and practical design method for skewed PMSMs. The proposed design method combines a small amount of 3-D-FEA with numerical calculations to shorten the development time while providing high accuracy.

The proposed method is explained using a design to reduce the THD of the induced voltage because one of the objectives herein is to evaluate the effect of voltage harmonics on experimental operation. Before starting the design, the designer determines the upper limit $M_{\rm max}$ of the number of steps M and the skew angle resolution $\theta_{\rm res}$, taking into consideration various factors, such as the expected manufacturing cost and stack length.

Fig. 7 shows the first step of the proposed method. First, in the investigated unskewed model, 2-D-FEA (or 3-D-FEA) is performed to obtain the original induced voltage including harmonics, as shown in Fig. 7(a). After obtaining the original voltage waveform, the unskewed model is divided axially into two units. As a result, the amplitude of the voltage waveform in each unit becomes half of the original one, as shown in Fig. 7(b). Next, the voltage waveform of one unit is shifted by the skew angle resolution $\theta_{\rm res}$ in the circumferential direction, and the waveform of the other unit is synthesized [Fig. 7(b)]. Consequently, a designer can roughly predict the voltage waveform after employing the step skew, as shown in Fig. 7(c). This process doubles the number of steps Min the investigated model because of the two axially divided units. With θ_{res} set to 1°, the THD of the composite voltage waveform is calculated for each 1° shift of the skew angle, and then this process is repeated until the θ_{res} with the lowest THD appears. Consequently, designers obtain a THD graph as a function of offset angle θ , as shown in Fig. 7(d). In this case, the THD is lowest at 20.0% when θ is 6°. After that, as shown in Fig. 8(a), each step of the model achieving the lowest THD is rearranged in one direction. Furthermore, steps having the same skew angle are combined, as shown in Fig. 8(b). Finally, 3-D-FEA is performed for the model reflecting the process shown in Fig. 8 to obtain an updated voltage waveform considering the skewing effect.

If the number of steps M has not reached $M_{\rm max}$ at this point, then the same procedure is repeated. The most important thing in this procedure is to perform 3-D-FEA again on the current model to compensate for the error in the voltage waveform before increasing the number of steps M. In particular, when skew is provided in an IPMSM, a large error occurs at the step skew angle $\theta_{\rm skew_step}$ because of leakage flux between steps. Therefore, to design a skewed PMSM with high accuracy, it is very effective to perform 3-D-FEA at this time. The same procedure is repeated using the voltage waveform obtained by 3-D-FEA, and the previous procedure is repeated until the number of steps M of all created models exceeds $M_{\rm max}$. Consequently, a model achieving a low THD with $M=M_{\rm max}$

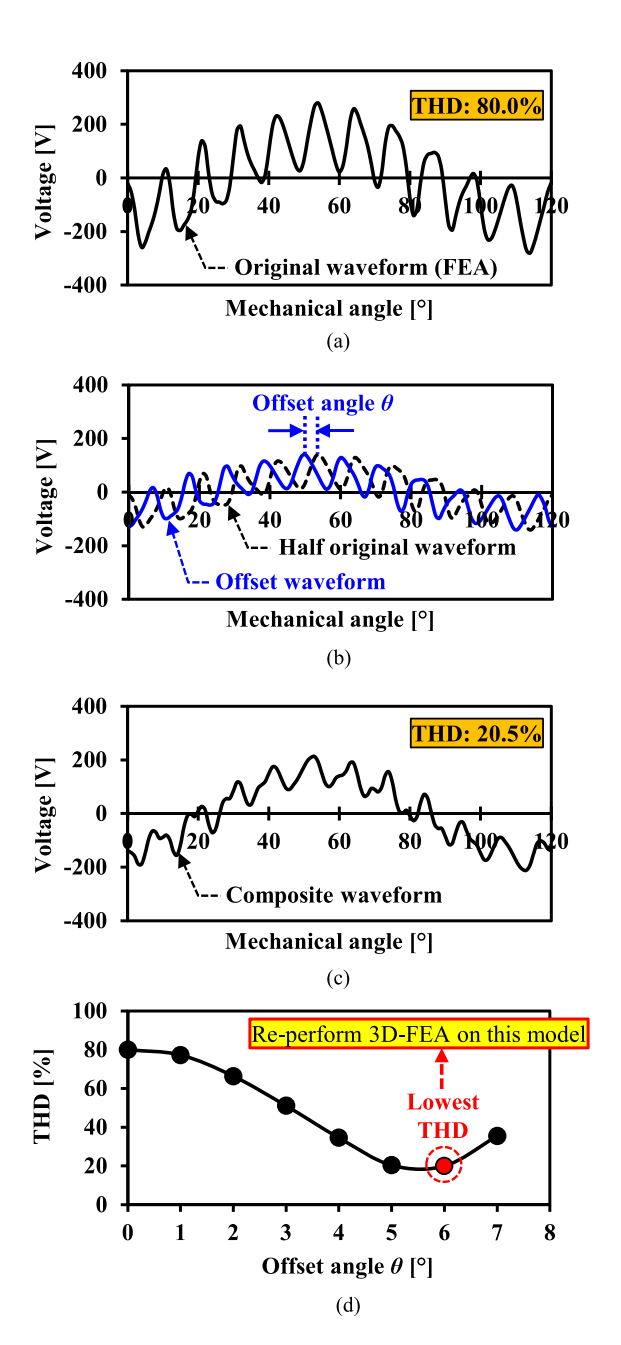


FIGURE 7. First step of the proposed design method: Synthesis of voltage waveforms and search for minimum THD. (a) Original voltage waveform. (b) Synthesis of voltage waveforms considering skew effect. (c) Composite voltage waveform ($\theta = 5^{\circ}$). (d) Calculated THDs vs. offset angle θ .

or less can be designed by performing 3-D-FEA just a few times.

Fig. 9 shows a flowchart summarizing the above procedure of the proposed design method. This article shows an example of reducing the THD of the voltage waveform, but the proposed method can also be applied to reducing torque ripple. In addition, the proposed method can be applied to any operating conditions and structure because errors are compensated for by limited 3-D-FEA. The necessity of compensating for errors during the design process using 3-D-FEA, as in the proposed

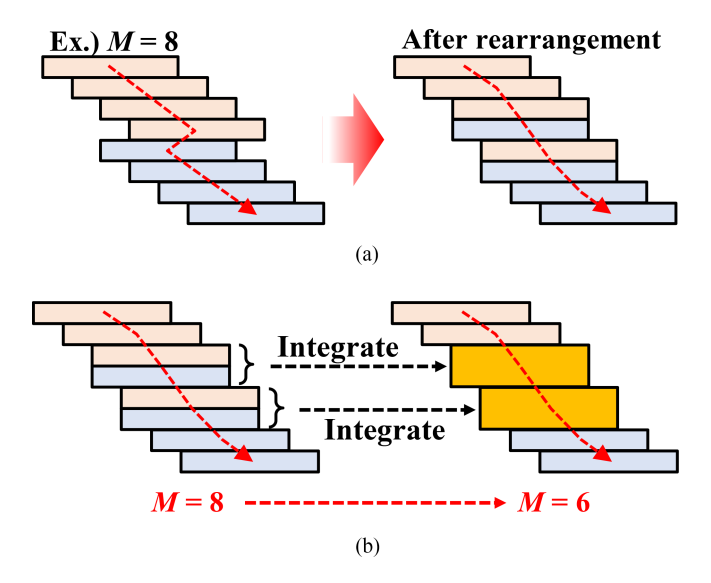


FIGURE 8. Second step of the proposed design method. (a) Rearrangement of each step. (b) Integration of steps having the same skew angle.

method, and the causes of errors are explained in the next subsection.

B. ERROR FACTORS IN DESIGNING SKEWED PMSMS

This subsection explains error factors in designing skewed PMSMs. Fig. 10 shows models and 3-D-FEA results with skew angles θ_{skew} of 2° and 5°, respectively. Fig. 10(a) shows the models and the observation lines of magnetic flux density. In the model with $\theta_{\text{skew}} = 5^{\circ}$, there is a gap between the magnets between the steps. Fig. 10(b) shows the axial magnetic flux density B_z on the observation line shown in Fig. 10(a) for both models. The evaluated operating point is 10 Arms, 7200 r/min, and $\beta = 70^{\circ}$. In the model with $\theta_{\text{skew}} = 5^{\circ}$, there are clearly four peaks, meaning that magnetic flux is leaking between the steps. In contrast, in the model with $\theta_{\text{skew}} = 2^{\circ}$, there is almost no leakage flux between the steps. Fig. 10(c) shows the locations where the four axial leakage flux peaks occur. Axial leakage flux occurs mainly between the parts where the permanent magnets or flux barriers overlap with the rotor core on another step because of the skew.

Fig. 11 shows the distribution of axial magnetic flux density B_z between steps for both models under the same operating point. In the model with $\theta_{\rm skew}=5^{\circ}$, axial leakage flux clearly occurs over a wide range. Therefore, as the skew angle $\theta_{\rm skew}$ increases, the axial leakage flux between steps could increase, leading to error, especially in IPMSMs.

Fig. 12 compares the error between calculated and 3-D-FEA predicted voltages for models with $\theta_{\rm skew}=2^{\circ}$ and 5° . Fig. 12(a) shows the voltage waveforms when $\theta_{\rm skew}=2^{\circ}$, and the calculation results and 3-D-FEA results match very well. In contrast, the voltage waveforms when $\theta_{\rm skew}=5^{\circ}$ in Fig. 12(b) have errors in places. This is due to the axial leakage flux between steps, as shown in Figs. 10 and 11. Fig. 12(c) compares the errors and shows that they are 1.2% and 34.4%

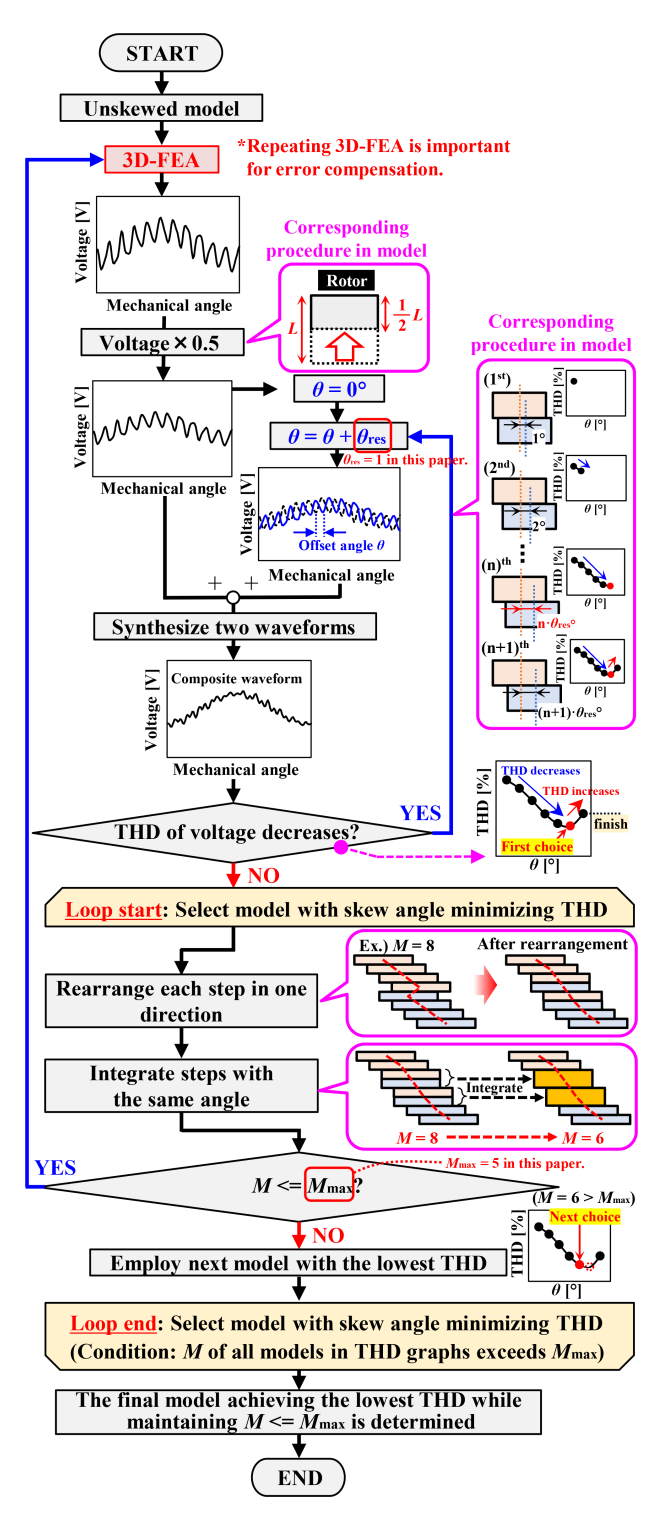


FIGURE 9. Flowchart of the proposed design method for skewed PMSM.

for $\theta_{\rm skew}=2^{\circ}$ and 5° , respectively, indicating that the error is more likely to occur when $\theta_{\rm skew}$ is large.

Accordingly, large errors can occur due to axial leakage flux depending on the conditions. Therefore, to design a skewed PMSM with high accuracy, it is extremely effective to correct errors with minimal 3-D-FEA, as in the proposed design method.

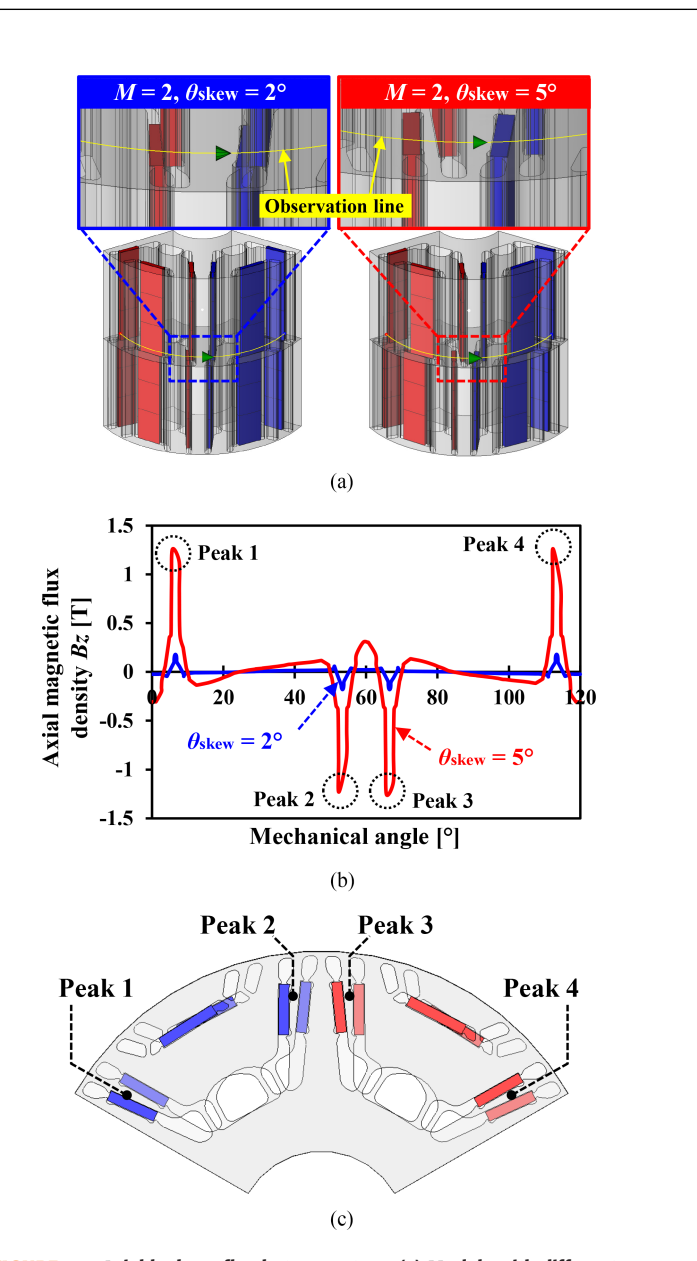


FIGURE 10. Axial leakage flux between steps. (a) Models with different skew angles. (b) Axial magnetic flux density B_z on the observation lines. (c) Corresponding areas with four peaks where peaks of axial leakage flux occur.

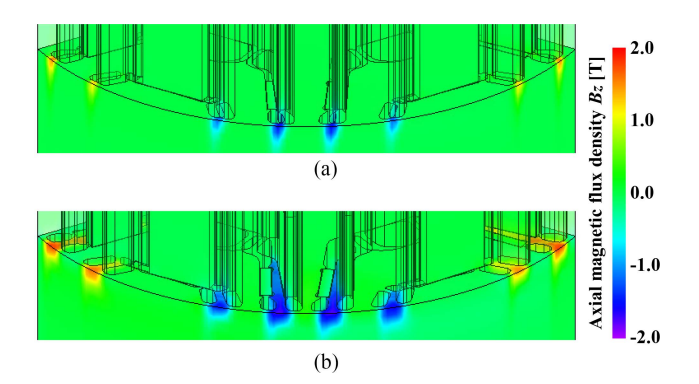
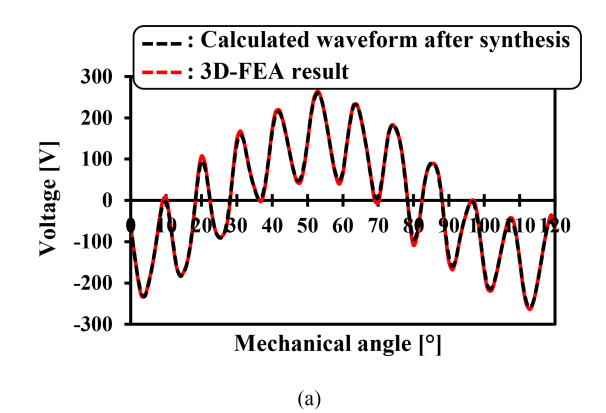
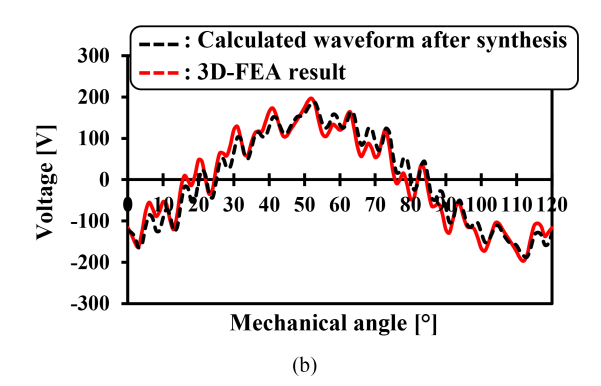


FIGURE 11. Distributions of axial magnetic flux density between steps at 7200 r/min, 10 Arms, and $\beta=70^\circ$. (a) $\theta_{\rm skew}=2^\circ$. (b) $\theta_{\rm skew}=5^\circ$.





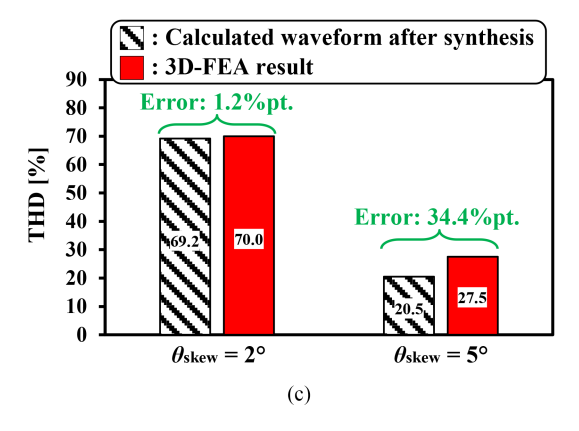


FIGURE 12. Error between calculated waveform and 3-D-FEA result for different skew angles $\theta_{\rm skew}$. (a) Voltage waveforms ($\theta_{\rm skew}=2^{\circ}$). (b) Voltage waveforms ($\theta_{\rm skew}=5^{\circ}$). (c) Comparison of errors.

C. DESIGN EXAMPLE USING PROPOSED METHOD

This subsection presents a design example using the proposed design method. The investigated model is the IPMSM shown in Fig. 1 and Table 2, and Table 3 lists the design conditions for this example. In general, the effect of reducing various harmonics is enhanced by increasing the number of steps M [6]. However, increasing the number of steps leads to reduced manufacturability. Accordingly, the upper limit $M_{\rm max}$ is set to 5 in this example. In addition, this example explores the skew structure that minimizes the THD of the voltage waveform during field-weakening control. Therefore, the operating conditions are a current of 10 Arms and a current phase angle β of 70° .

TABLE 3. Example of Design Conditions in the Proposed Method

Item	Value	
Offset angle resolution $ heta_{ m res}$	1°	
Maximum No. of steps M_{max}	5 steps	
Target operating point	10 Arms, $\beta = 70^{\circ}$	

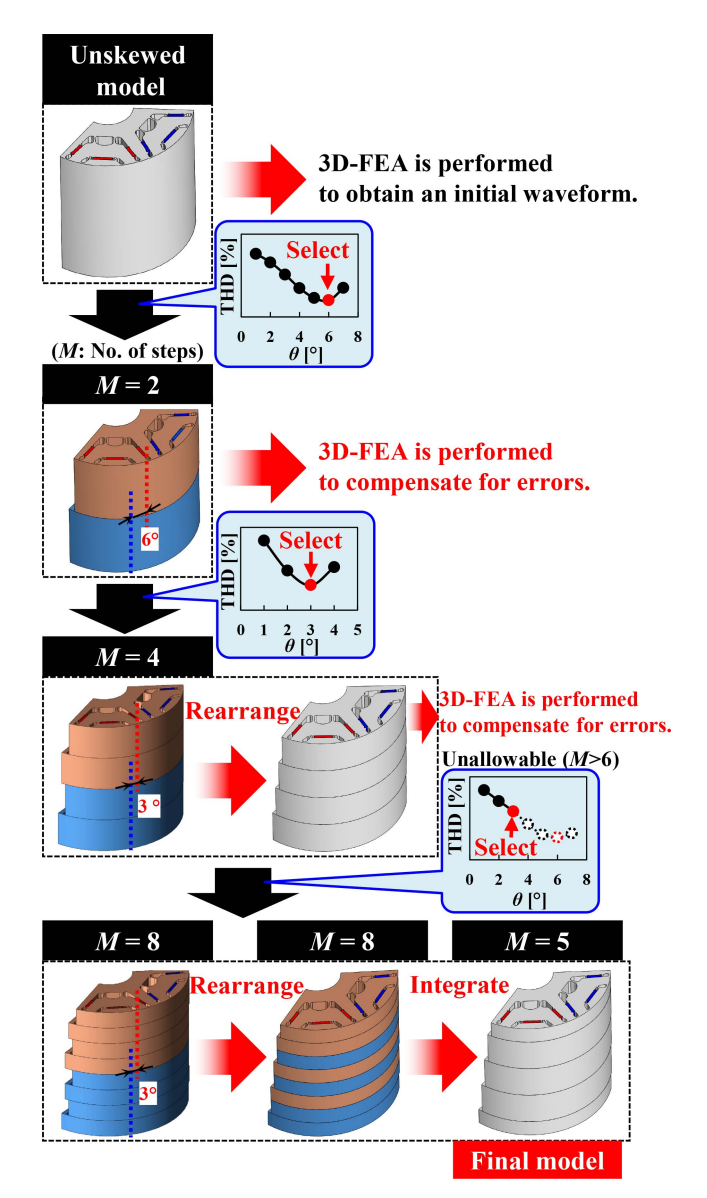


FIGURE 13. Evolution of skewed model when designed under the conditions in Table 3.

Fig. 13 shows the evolution of the skewed model when designed under the conditions in Table 3. First, the voltage waveform of the unskewed model is used to search for a model with the minimum THD when M = 2, and 3-D-FEA is performed on that model to compensate for the error. That voltage waveform is used to search for a model with the

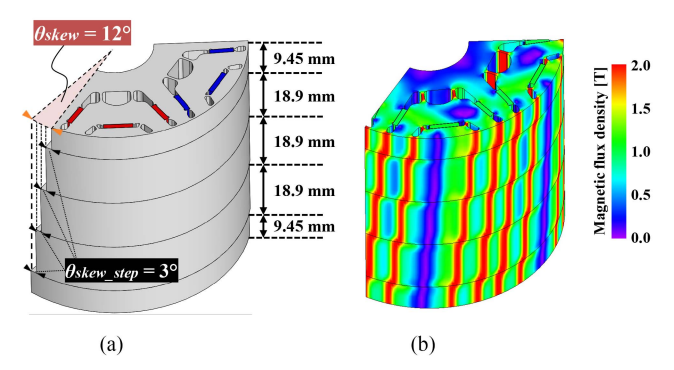


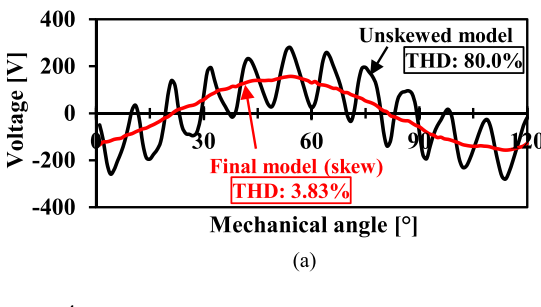
FIGURE 14. Final model designed based on the proposed method with design conditions shown in Table 3. (a) Model and dimensions. (b) Magnetic flux density distributions (7200 r/min, 10 Arms, and $\beta = 70^{\circ}$).

minimum THD when M = 4. After running 3-D-FEA again, the same procedure is repeated with M = 8. At this point, although M_{max} is exceeded, the designer investigates whether there is a pattern in which M can be made below M_{max} by integrating steps with the same skew angle. In this example, a model with M = 5 exists and has a lower THD than any model with M = 4, so that model is selected as the final model, as shown in Fig. 13.

Fig. 14 shows the designed final model with step skew based on the proposed design method. As shown in Fig. 14(a), the final model has M=5 steps. The heights of some steps are different because steps with the same skew angle are combined. The final model has a total skew angle $\theta_{\rm skew}$ of 12°. In this example, only four 3-D-FEA simulations were required to arrive at the final model, which is a very small number of simulations to reveal the effective step skewed structure. In addition, even a novice can design a high-performance skewed PMSM without using complex formulas or theories by using this design method. Fig. 14(b) shows the magnetic flux density in the final model at the investigated operating point.

Fig. 15 describes the effect of the step skewed structure obtained by the proposed method on the voltage and torque waveforms. As shown in Fig. 15(a), the final skewed model achieves a much lower THD of 3.83% than that of the unskewed model (80%). The skewed model also effectively improves the torque ripple as shown in Fig. 15(b), reducing it from 85.3% in the unskewed model to 4.28%. In summary, the final skewed model designed by the proposed design method can, respectively, reduce the torque ripple and voltage THD by approximately 80% from the original model without skew.

As mentioned above, Fig. 2 searches for a model with the lowest THD through parametric study. Fig. 16 compares the THD and torque ripple of the final model designed using the proposed method and the conventional step skew, demonstrating the effectiveness of the proposed method. Even the conventional step skew designed by parametric study can effectively reduce harmonics compared to the model without skew. The final skewed model designed by the proposed



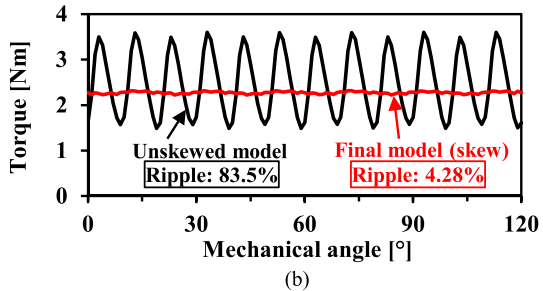
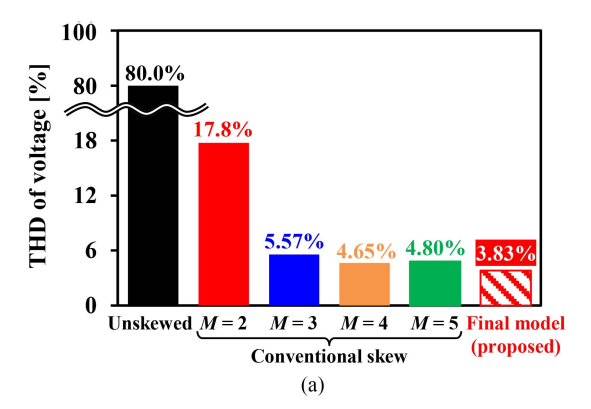


FIGURE 15. Voltage and torque waveforms between unskewed model and final skewed model at 7200 r/min and 10 Arms. (a) Voltage waveform. (b) Torque waveform.



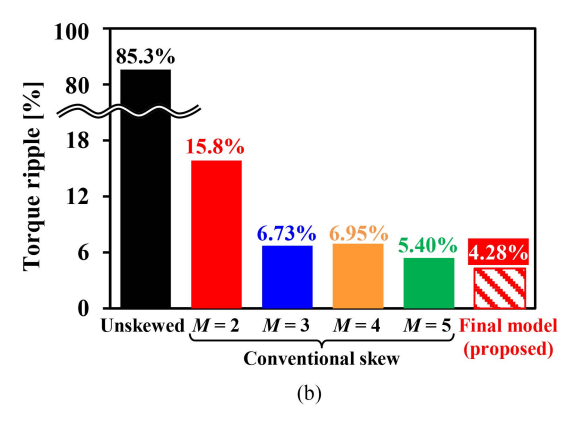
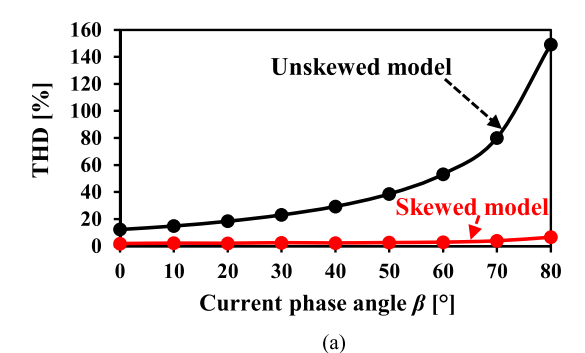


FIGURE 16. Comparison of THD and torque ripple between models using conventional skew obtained by parametric study and proposed skewed model under field-weakening control at 7200 r/min and 10 Arms. (a) THD. (b) Torque ripple.



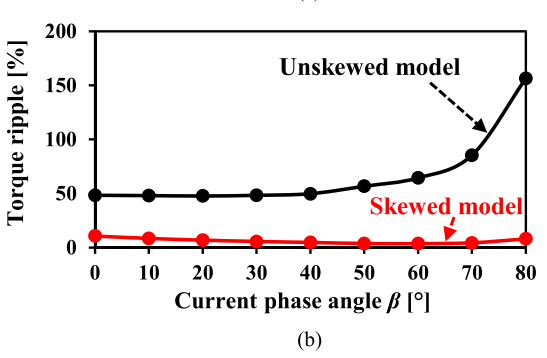


FIGURE 17. Voltage THD and torque ripple of the final model and unskewed model when changing current phase angle β at 7200 r/min and 10 Arms. (a) THD. (b) Torque ripple.

method has further reduced the THD and torque ripple. Therefore, the design method proposed in this article can not only shorten the development time but also improve the performance of step skew.

Fig. 17 shows the voltage THD and torque ripple of the final model and the unskewed model when the current phase angle β is changed. In the unskewed model, the THD and torque ripple increase rapidly as the current phase angle β increases. In contrast, the final model employing skew is designed using a waveform of $\beta = 70^{\circ}$, and hence both the THD and torque ripple are much lower than in the unskewed model. In addition, the final model shows a high reduction effect on the torque ripple and voltage THD at any current phase angle β .

This article presents an optimal design with current phase angle $\beta=70^{\circ}$ to suppress voltage harmonics in order to investigate the impact on experimental operation. When using the proposed method, the operating conditions to be optimized are selected depending on the application and the designer. For example, in the case of a traction motor, it would be effective to apply the proposed method in frequently used operating area in the WLTC operating mode, etc.

IV. ACCURACY AND ANALYSIS TIME OF THE PROPOSED DESIGN METHOD

A. EVALUATION OF ACCURACY USING CASE STUDIES

This subsection explains the importance of compensating for errors using 3-D-FEA during the design process in the

TABLE 4. Design Conditions of Three Case Studies

Conditions	Case 1	Case 2	Case 3
Model (No. of poles / slots)	6p/36s	6p/18s	6p/18s
Offset angle resolution $ heta_{ m res}$	1°	1°	1°
Maximum No. of steps M_{max}	5 steps	5 steps	8 steps

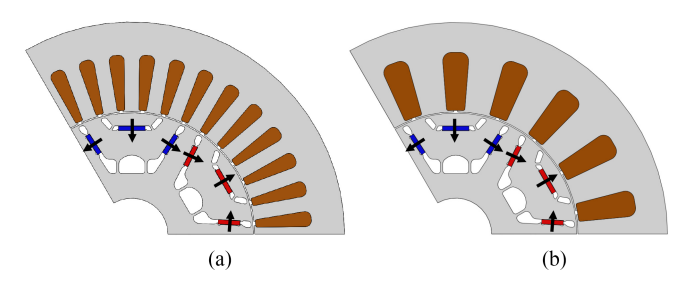
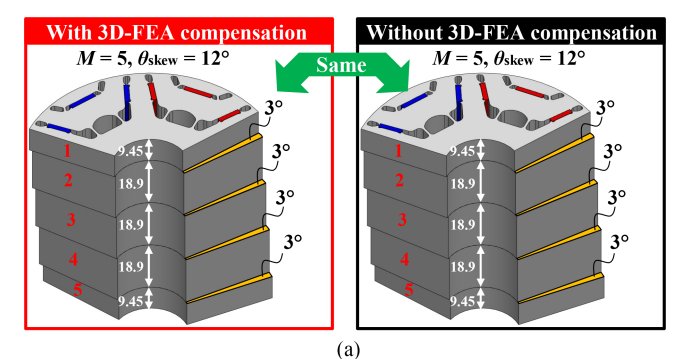


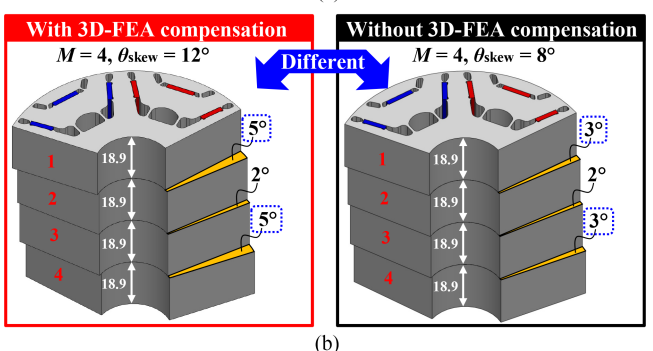
FIGURE 18. Cross-sectional views of two investigated IPMSMs. (a) 6-pole and 36-slot model. (b) 6-pole and 18-slot model.

proposed design method, as shown in Fig. 9, through three case studies. As shown in Table 4, the number of slots N_s of the IPMSM and the design constraints are changed in three cases, and the impact on accuracy of whether error compensation is used during the design process using 3-D-FEA is evaluated. Fig. 18 shows models with $N_s = 36$ and 18, and the same rotor with six poles is used. Case 1 corresponds to the same conditions as in the previous section as shown in Table 3. In Case 2, the number of slots is changed to 18, but the skew angle resolution $\theta_{\rm res}$ and maximum number of steps $M_{\rm max}$ are the same as in Case 1. Case 3 has the same 18-slot model as in Case 2, but the maximum number of steps $M_{\rm max}$ is increased to 8.

Fig. 19 compares the final models in three case studies when a skewed IPMSM is designed using the proposed method, and when error compensation is and is not performed during the design process using 3-D-FEA. In Case 1 in Fig. 19(a), the exact same final model is obtained by chance regardless of whether error compensation is performed by 3-D-FEA. This is thought to be due to the fact that the theoretical skew angle is relatively small at 10 ° based on (1).

In Case 2 in Fig. 19(b), the skew angle of the final model differs depending on whether error compensation is performed by 3-D-FEA. This means that if the error in the numerical calculation becomes large during the design, then the error will accumulate when the waveform is used without error compensation by 3-D-FEA and the next process is carried out. In addition, the number of slots is changed to 18, so the theoretical skew angle according to (1) is 20° . As a result, the step skew angle $\theta_{\text{skew_step}}$ is likely to become large, and axial leakage flux is likely to occur. Therefore, the likelihood of error occurring differs depending on the combination of the number of poles and slots. In addition, in Case 3 in Fig. 19(c), not only the skew angle of the final model but also the number of steps M differs depending on whether error compensation is performed by 3-D-FEA.





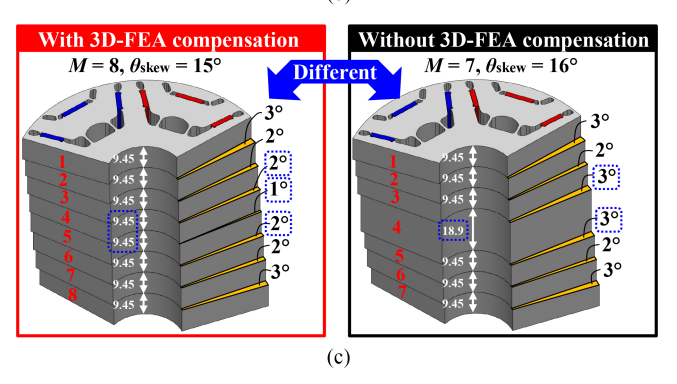


FIGURE 19. Comparison of final models with and without error compensation during the design process using 3-D-FEA. (a) Case 1. (b) Case 2. (c) Case 3.

Figs. 20–22 show comparisons between voltage waveforms of the final model calculated by the flowchart and predicted by FEA with and without error compensation by 3-D-FEA in Cases 1–3, respectively. In Case 1 shown in Fig. 20, since the final model obtained is the same regardless of whether error compensation is used, as shown in Fig. 19(a), so the FEA-predicted waveforms in Fig. 20(a) and (b) are also the same. However, the waveforms that are the final calculation results in the flowchart and their THDs are different. Therefore, although the structure of the final model does not change depending on whether error compensation is performed by 3-D-FEA, the final predicted waveforms are different.

In Case 2 shown in Fig. 21, the THD of the waveform obtained by the calculation is lower in Fig. 21(a), where error compensation is performed by 3-D-FEA. In addition, the voltage waveform obtained by 3-D-FEA of the final model also shows almost the same THD and is highly accurate. However, when error compensation is not performed as in Fig. 21(b),

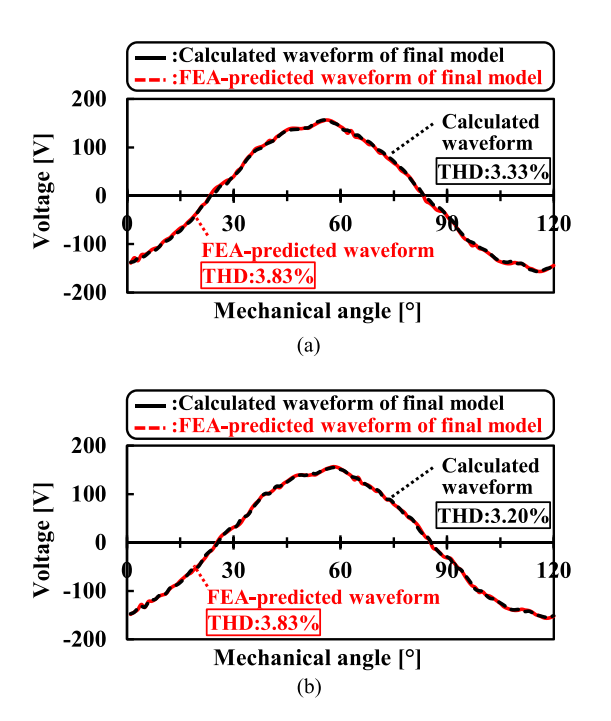


FIGURE 20. Comparison of voltage waveforms calculated by flowchart and predicted by FEA for the final model in Case 1. (a) With 3-D-FEA compensation. (b) Without 3-D-FEA compensation.

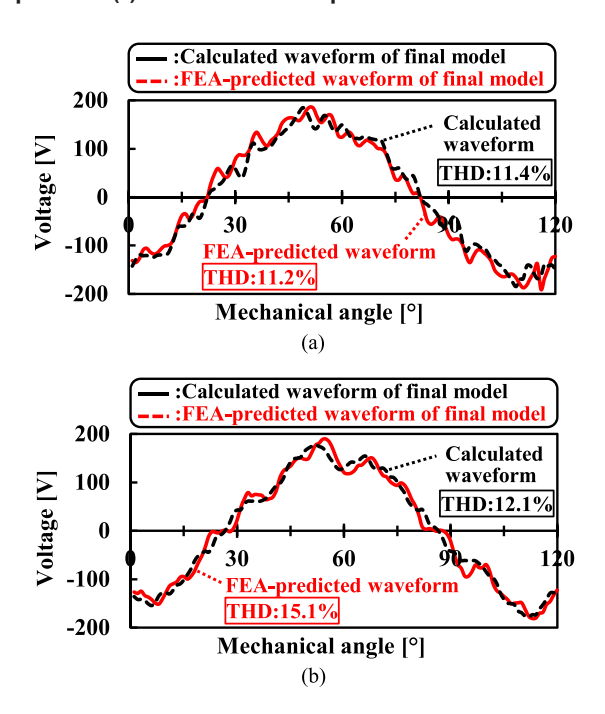


FIGURE 21. Comparison of voltage waveforms calculated by flowchart and predicted by FEA for the final model in Case 2. (a) With 3-D-FEA compensation. (b) Without 3-D-FEA compensation.

then when the voltage waveform is actually analyzed by 3-D-FEA, the THD is higher than that of the final calculation result waveform. In Case 3 shown in Fig. 22, the THD is higher in the waveform calculated by the flowchart when error compensation is performed as in Fig. 22(a). However, when the waveform of the actual model is checked with 3-D-FEA,

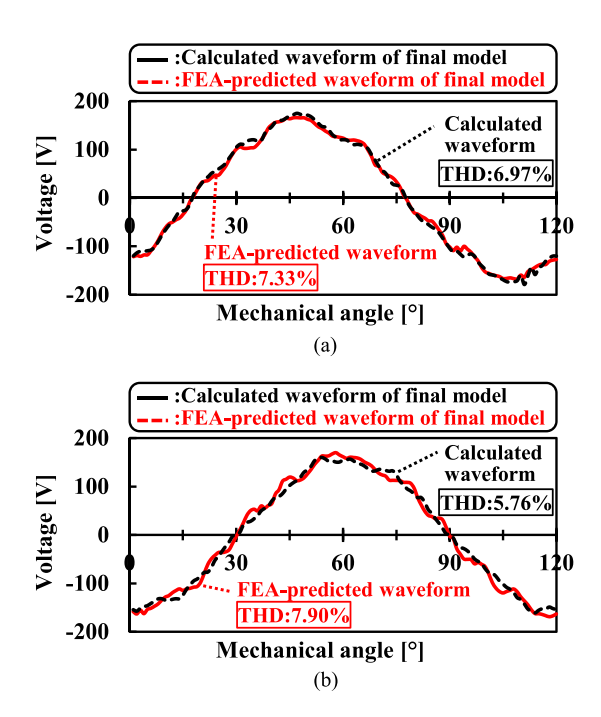


FIGURE 22. Comparison of voltage waveforms calculated by flowchart and predicted by FEA for the final model in Case 3. (a) With 3-D-FEA compensation. (b) Without 3-D-FEA compensation.

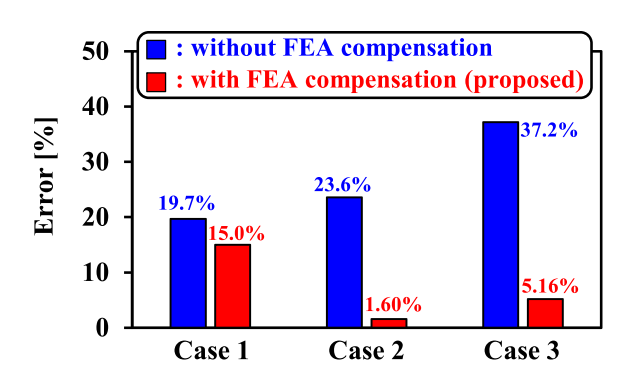


FIGURE 23. Summary of THD error ratios of the waveforms in Figs. 15–17.

the THD increases in Fig. 22(b), where error compensation is not performed because of the large error, and the final model THD is higher.

Fig. 23 summarizes the THD error ratios of the waveforms in Figs. 20–22. In all cases, error compensation using 3-D-FEA can improve the accuracy of the voltage waveform obtained in the final model. In particular, in the 18-slot model, the theoretical skew angle $\theta_{\rm skew_theo}$ calculated by (1) is larger than that in the 36-slot model, so the step skew angle $\theta_{\rm skew_step}$ during the calculation is also larger. As a result, as shown in Figs. 10–12, the leakage flux between steps in the axial direction increases, and the error increases when only numerical calculation is used. However, by using the 3-D-FEA compensation, it is possible to accurately predict the voltage waveform even in such a case. Consequently, the proposed

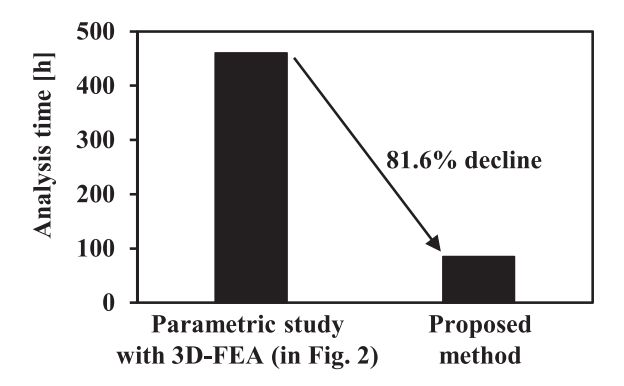


FIGURE 24. Comparison of analysis time between parametric study and proposed design method.

method performs a minimal amount of 3-D-FEA, making it possible to design a skewed PMSM with high robustness and high accuracy under various conditions.

B. ANALYSIS TIME OF THE PROPOSED METHOD

Fig. 24 compares the analysis time by 3-D-FEA when the optimal skew model is designed within $M_{\rm max}=5$ in both the parametric study and the proposed design method. The parametric study employs a full search with varying skew angle and step number M, as shown in Fig. 2. Designing a skewed IPMSM using the proposed design method not only further reduces the THD and torque ripple but also reduces the analysis time by 81.6% compared with the parametric study. This is because as mentioned above, 3-D-FEA is only performed for error compensation during the design process and is performed a minimal number of times. As described above, the proposed design method makes it possible to design a high-performance skewed PMSM simply, quickly, and accurately.

V. EXPERIMENTAL RESULTS FOR A DESIGNED IPMSM

This section uses a prototype to verify the skewed IPMSM designed by the proposed design method. The unskewed and skewed rotors are compared to evaluate the effect of skew in the experiment. Fig. 25 shows each component of the prototypes. Fig. 25(a) and (b) show the unskewed and skewed rotors, where the skewed rotor was designed using Case 1 of the proposed design method. Fig. 25(c) shows the rotor core of each step of the skewed rotor. The step skew is achieved by changing the key angle by 3° at each step. Fig. 25(d) shows the assembled rotor with the step skew, and Fig. 25(e) shows the 36-slot stator.

Fig. 26 compares the induced voltage waveforms obtained by analysis and experiment at no load for the two rotors. In both the unskewed and skewed rotors, the 3-D-FEA and experimental results are in excellent agreement. This implies that the accuracy of the 3-D-FEA is also high, and the proposed design method, which compensates for the error, can predict the performance of the actual machine with high accuracy. In addition, the voltage waveform in Fig. 26(b) obtained

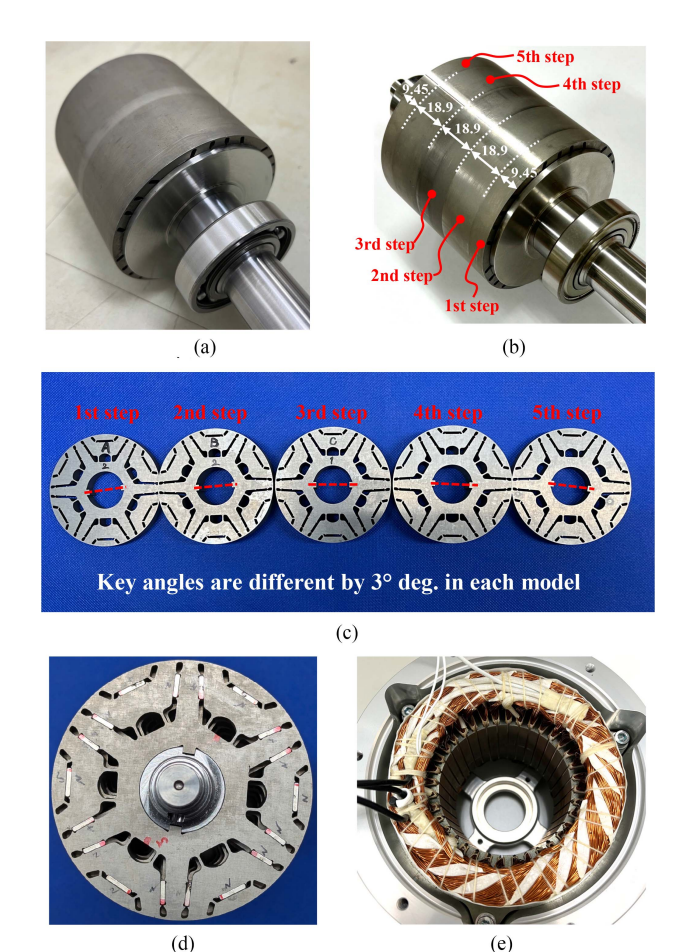


FIGURE 25. Prototypes of unskewed and skewed IPMSMs. (a) Unskewed rotor. (b) Skewed rotor designed by proposed method. (c) Each step of rotor core in skewed rotor. (d) Top view of assembly of skewed rotor. (e) Common stator.

by the proposed design method achieves very low THD even in the actual machine, and a high skew effect is obtained.

Fig. 27 shows the change in average torque versus current phase angle β at maximum current for the two rotors. Reluctance torque occurs in addition to magnet torque because both are IPMSMs. Furthermore, the trends in the analysis results and experimental results for both rotors agree well. Although the skewed rotor has a slight decrease in average torque, this is due to a decrease in the winding factor caused by the skew.

Fig. 28 shows measured line-to-line voltage waveforms when 10 Arms is applied with pulsewidth modulation (PWM) drive by an inverter for the unskewed and skewed rotors, respectively. The current phase angle β is 70°, and field-weakening control is applied. During PWM drive, a high-frequency voltage equivalent to the switching frequency is superimposed, making it difficult to evaluate the slot harmonics of the induced voltage. Therefore, in Fig. 28, a low-pass filter (LPF) with a cutoff frequency of 3 kHz is applied to the measuring instrument. When the slot harmonics are close to the cutoff frequency, they are attenuated. Accordingly, the

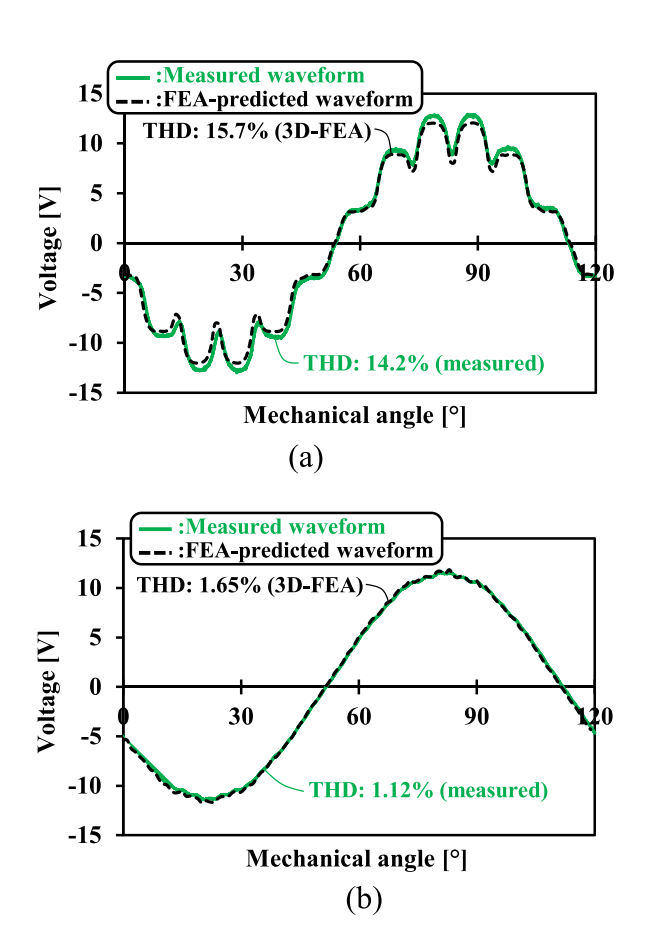


FIGURE 26. Comparison of induced voltage waveforms obtained by analysis and experiment at no-load for the two rotors. (a) Unskewed rotor. (b) Skewed rotor.

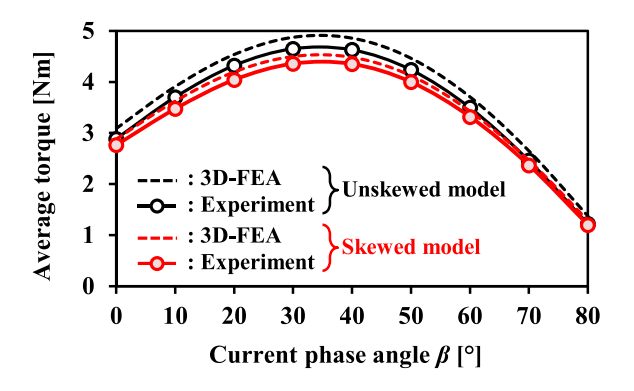
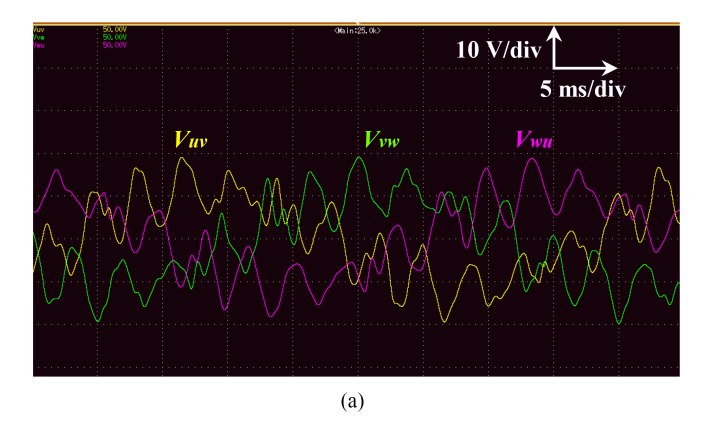


FIGURE 27. Measured and FEA-predicted torque characteristics versus current phase angle.

induced voltages shown in Fig. 28 are evaluated at a low speed of 500 r/min.

In case of the unskewed rotor shown in Fig. 28(a), large slot harmonics are obviously superimposed on the induced voltage. In contrast, the skewed rotor suppresses the slot harmonics, as shown in Fig. 28(b). The THD of the respective voltage waveforms is 65.5% and 13.8%. On the other hand, the voltage during on-load condition with the inverter is affected by various factors, such as control, LPF, and measuring



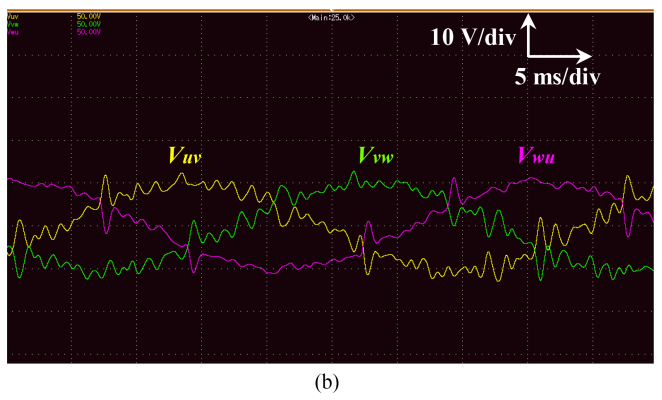


FIGURE 28. Measured line-to-line voltage during PWM drive with LPF applied (500 r/min, 10 Arms, and $\beta=70^{\circ}$). (a) Unskewed rotor. (b) Skewed rotor.

instruments, making the error large. However, these results demonstrate that the skew can suppress the slot harmonics in actual machines.

Fig. 29 shows measured input current when the rated armature current of 10 Arms with a current phase angle β of 70° is applied. In the unskewed rotor, the input current includes the slot harmonics, resulting in a high THD of 7.64%. This means that the slot harmonics in the induced voltage causes the harmonic current. In contrast, the input current of the skewed machine is an almost sinusoidal waveform because the THD is 0.70%. This low THD of the input current is obtained by low slot harmonics in the induced voltage. Accordingly, these results imply that the slot harmonics of the induced voltage increase the iron loss. The skewed machine designed by the proposed method contributes to improving the quality of the current control.

Fig. 30 shows the THD of input current when the current phase angle β is changed at 7200 r/min and 10 Arms. The THD of input current to the unskewed model increases as the current phase angle increases because the voltage harmonics also increase, as shown in Fig. 17(a). In contrast, the THD of input current to the skewed machine is not strongly affected by the current phase angle because the voltage harmonics are much smaller than in the unskewed model. Hence, the skewed machine can operate with input current close to a sinewave regardless of the operating conditions.

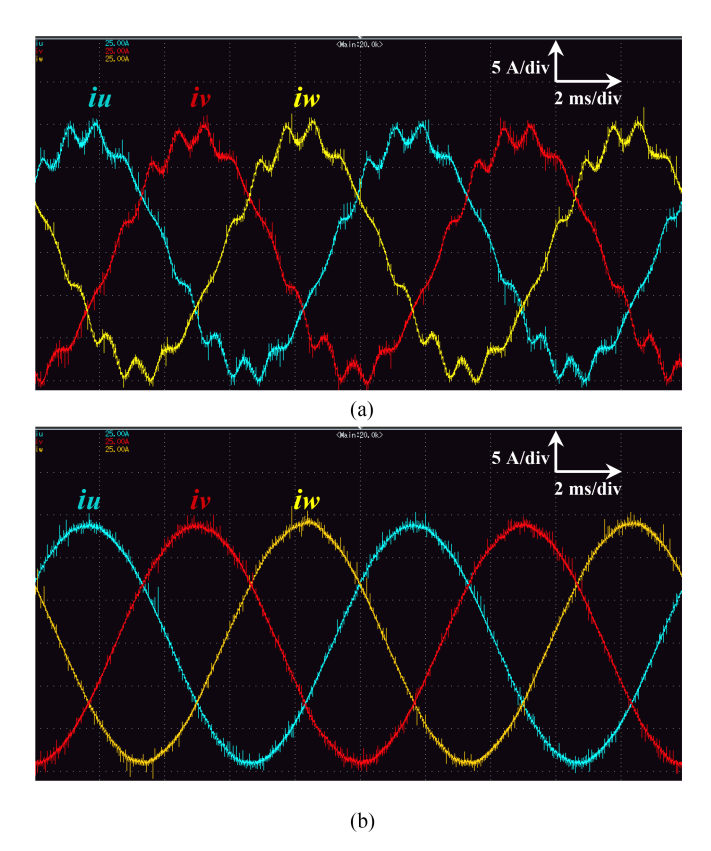


FIGURE 29. Measured input current during PWM drive (7200 r/min, 10 Arms, and $\beta = 70^{\circ}$). (a) Unskewed rotor. (b) Skewed rotor.

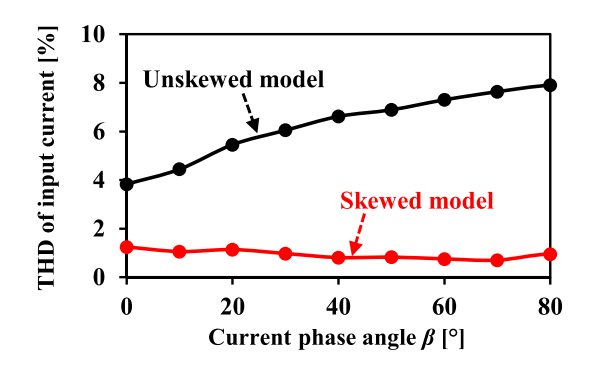


FIGURE 30. THD of input current against current phase angle β at 7200 r/min and 10 Arms.

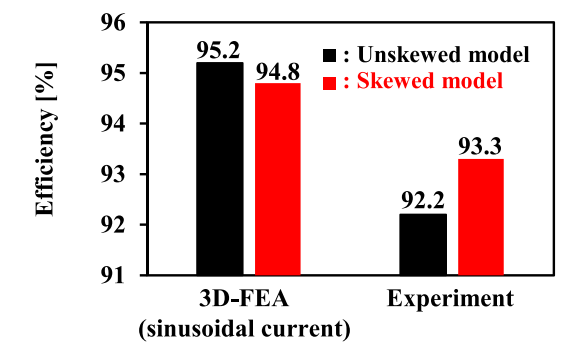


FIGURE 31. Comparison of efficiency between 3-D-FEA and measured values at 7200 r/min, 10 Arms, and $\beta = 70^{\circ}$.

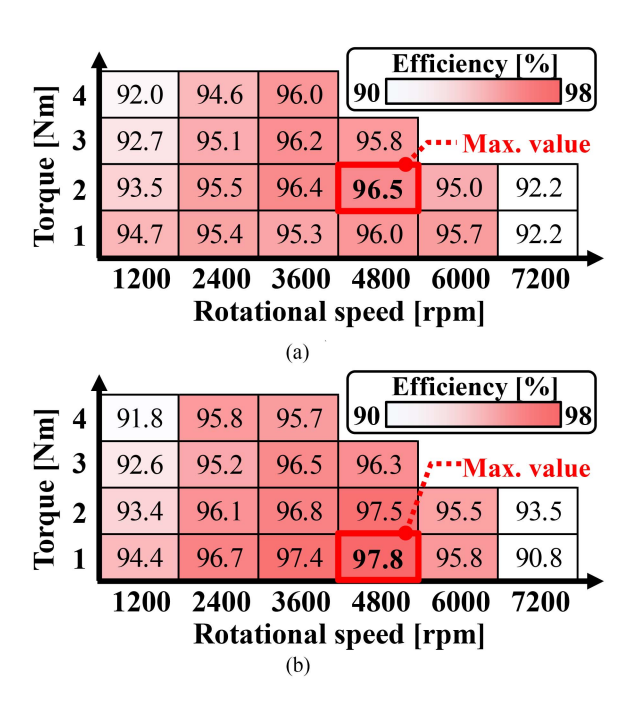


FIGURE 32. Measured efficiency maps. (a) Unskewed rotor. (b) Skewed rotor.

Fig. 31 shows a comparison of efficiency between 3-D-FEA and measured values in both machines at the operating point of 7200 r/min, 10 Arms, and $\beta = 70^{\circ}$. In terms of the 3-D-FEA results, the unskewed machine shows superior efficiency to the skewed machine. However, in experiments, the skewed machine shows higher efficiency than that of the unskewed machine. This is because the efficiency of the unskewed machine is reduced dramatically by the harmonic current caused by the induced voltage, as shown in Fig. 29(a). The skewed machine can suppress an increase in the iron loss caused by harmonic current in experiments. As a result, the superiority of the efficiency in both machines is reversed between 3-D-FEA and experiment. Consequently, using skew to reduce the voltage harmonics is effective in improving the efficiency at the target operating point.

Fig. 32 compares the efficiency maps measured over a wide range for both models. The efficiency of the skewed model is higher over a wider range than the unskewed model because input current harmonics can be reduced. The efficiency improvement effect is particularly significant in regions where iron loss is dominant, such as light loads. The maximum efficiency of the skewed model is 97.8%, an improvement over 96.5% of the unskewed model.

VI. CONCLUSION

This article proposed a time-efficient, practical, and simple design method that can quickly and accurately construct an appropriate skewed PMSM. The proposed method combines simple numerical calculations with a minimal amount of 3-D-FEA. Because errors are compensated for by 3-D-FEA during the numerical calculation process, it can be applied to any motor structure and is highly robust. In addition, the numerical

calculations are simple and can be easily implemented in environments, such as Excel and MATLAB, making it practical. Although this article showed an example of reducing the voltage THD of an IPMSM, the same can be applied to reducing torque ripple. The IPMSM designed using the proposed method realized lower THD than that of a conventional skewed machine. In addition, although the constraint condition was the number of steps M, various other applications are also possible, such as changing the constraint to the value of THD or torque ripple.

In addition, this article revealed how the slot harmonics affect the operating characteristics. The slot harmonics of the induced voltage cause the harmonics of input current during PWM drive. As a result, the skewed IPMSM with small slot voltage harmonics can realize high-quality current control, contributing to improved efficiency.

REFERENCES

- S. Liu, H. Wu, T. Bosma, and X. Wang, "Impact of DC-link voltage control on torsional vibrations in grid-forming PMSG wind turbines," *IEEE Trans. Energy Convers.*, vol. 39, no. 4, pp. 2631–2642, Dec. 2024.
- [2] M. S. Baumann, A. Steinboeck, W. Kemmetmüller, and A. Kugi, "Real-time capable thermal model of an automotive permanent magnet synchronous machine," *IEEE Open J. Ind. Electron. Soc.*, vol. 5, pp. 501–516, 2024.
- [3] D. Wang, X. Wang, and S.-Y. Jung, "Cogging torque minimization and torque ripple suppression in surface-mounted permanent magnet synchronous machines using different magnet widths," *IEEE Trans. Magn.*, vol. 49, no. 5, pp. 2295–2298, May 2013.
- [4] W. Q. Chu and Z. Q. Zhu, "Investigation of torque ripples in permanent magnet synchronous machines with skewing," *IEEE Trans. Magn.*, vol. 49, no. 3, pp. 1211–1220, Mar. 2013.
- [5] G. Jungmayr, J. Loeffler, B. Winter, F. Jeske, and W. Amrhein, "Magnetic gear: Radial force, cogging torque, skewing, and optimization," *IEEE Trans. Ind. Appl.*, vol. 52, no. 5, pp. 3822–3830, Sep./Oct. 2016.
- [6] R. Tsunata and M. Takemoto, "Skewing technology for permanent magnet synchronous motors: A comprehensive review and recent trends," *IEEE Open J. Ind. Electron. Soc.*, vol. 5, pp. 1251–1273, 2024.
- [7] H.-W. Yang, D. H. Kang, S.-G. Kang, D. Jang, S.-W. Jung, and S.-Y. Jung, "Analysis of skewing method considering 3-D electromagnetic force," in *Proc. IEEE 20th Biennial Conf. Electromagn. Field Computation*, 2022, pp. 1–2.
- [8] R. P. Deodhar, D. A. Staton, and T. J. E. Miller, "Modelling of skew using the flux-MMF diagram," in *Proc. Int. Conf. Power Electron.*, *Drives Energy Syst. Ind. Growth*, 1996, pp. 546–551.
- [9] I.-S. Jung, J. Hur, and D. -S. Hyun, "3-D analysis of permanent magnet linear synchronous motor with magnet arrangement using equivalent magnetic circuit network method," *IEEE Trans. Magn.*, vol. 35, no. 5, pp. 3736–3738, Sep. 1999.
- [10] D. J. Gómez, A. Tovar-Barranco, A. L. Rodríguez, A. López-de-Heredia, and I. Villar, "On-load cogging torque calculation using frozen permeability method and permeance network models," in *Proc. 22th Int. Conf. Elect. Machines*, 2016, pp. 499–505.
- [11] D. Gerling, "Analytical calculation of the PM machine magnetic field depending on magnet width and skewing," in *Proc. 13th Eur. Conf. Power Electron. Appl.*, 2009, pp. 1–7.
- [12] M.-M. Koo, S.-M. Jang, Y.-S. Park, H.-I. Park, and J.-Y. Choi, "Characteristic analysis of direct-drive wind power generator considering permanent magnet shape and skew effects to reduce torque ripple based on analytical approach," *IEEE Trans. Magn.*, vol. 49, no. 7, pp. 3917–3920, Jul. 2013.

- [13] L. Xue, L. Luo, Y. Gu, C. Chen, and Y. Li, "Analytical calculation and analysis of electromagnetic torque for a skewed brushless DC motor with halbach array," in *Proc. 20th Int. Conf. Elect. Machines Syst.*, 2017, pp. 1–6.
- [14] S. Nian, L. Zhu, X. Luo, and Z. Huang, "Analytical methods for optimal rotor step-skewing to minimize cogging torque in permanent magnet motors," in *Proc. 22nd Int. Conf. Elect. Machines Syst.*, 2019, pp. 1–5.
- [15] Y. An et al., "Calculation model of armature reaction magnetic field of interior permanent magnet synchronous motor with segmented skewed poles," *IEEE Trans. Energy Convers.*, vol. 37, no. 2, pp. 1115–1123, Jun. 2022.
- [16] S. Zhang and S. Guo, "An analytical method for electromagnetic performance calculation in surface-mounted permanent-magnet machines with skewing," in *Proc. 21st Int. Conf. Elect. Machines Syst.*, 2018, pp. 2697–2701.
- [17] S. Zhao, J. Chen, Y. Gao, and C. Zhang, "Fast calculation of electromagnetic force and vibration for surface mounted PMSM considering spatial harmonic suppression," in *Proc. 26th Int. Conf. Elect. Machines Syst.*, 2023, pp. 1184–1189.
- [18] Y. An et al., "Open-circuit air-gap magnetic field calculation of interior permanent magnet synchronous motor with V-shaped segmented skewed poles using hybrid analytical method," *IEEE Trans. Magn.*, vol. 57, no. 12, Dec. 2021, Art. no. 8108309.
- [19] G. Y. Sizov et al., "Modeling and analysis of effects of skew on torque ripple and stator tooth forces in permanent magnet AC machines," in *Proc. IEEE Energy Convers. Congr. Expo.*, 2012, pp. 3055–3061.
- [20] M. Mohr, O. Bíró, A. Stermecki, and F. Diwoky, "A finite element-based circuit model approach for skewed electrical machines," *IEEE Trans. Magn.*, vol. 50, no. 2, pp. 837–840, Feb. 2014.
- [21] M. Jaeger, S. Rick, and K. Hameyer, "Current simulation of a controlled PMSM including skew and torsional rotor vibrations," in *Proc. 13th Int. Conf. Elect. Machines*, 2018, pp. 111–117.
- [22] P. Lazari, B. Sen, J. Wang, and X. Chen, "Accurate D-Q axis modeling of synchronous machines with skew accounting for saturation," *IEEE Trans. Magn.*, vol. 50, no. 11, Nov. 2014, Art. no. 8105704.
- [23] M. Elamin and P. Wendling, "NVH analysis of rotor step skewing on permanent magnet synchronous motor," in *Proc. IEEE Transp. Electrific. Conf. Expo*, 2022, pp. 796–800.
- [24] J. Urresty, J. Riba, H. Saavedra, and J. Romeral, "Analysis of demagnetization faults in surface-mounted permanent magnet synchronous motors with symmetric windings," in *Proc. 8th IEEE Symp. Diagnostics Elect. Machines, Power Electron. Drives*, 2011, pp. 240–245.
- [25] H. Jang, H. Kim, D.-W. Nam, W.-H. Kim, J. Lee, and C. Jin, "Investigation and analysis of novel skewing in a 140 kW traction motor of railway cars that accommodate limited inverter switching frequency and totally enclosed cooling system," *IEEE Access*, vol. 9, pp. 121405–121413, 2021.
- [26] P. Lazari, J. Wang, and B. Sen, "3-D effects of rotor step-skews in permanent magnet-assisted synchronous reluctance machines," *IEEE Trans. Magn.*, vol. 51, no. 11, Nov. 2015, Art. no. 8112704.
- [27] M. Klausnitzer and A. Moeckel, "Methods for calculation of skewed permanent magnet motors for short and highly saturated motors," in *Proc. Innov. Small Drives Micro-Motor Syst.*; 9. GMM/ETG Symp., 2013, pp. 1–5.
- [28] M. Lukaniszyn, M. JagieLa, and R. Wrobel, "Optimization of permanent magnet shape for minimum cogging torque using a genetic algorithm," *IEEE Trans. Magn.*, vol. 40, no. 2, pp. 1228–1231, Mar. 2004.
- [29] A. Mahmoudi, S. Kahourzade, N. A. Rahim, and W. P. Hew, "Design, analysis, and prototyping of an axial-flux permanent magnet motor based on genetic algorithm and finite-element analysis," *IEEE Trans. Magn.*, vol. 49, no. 4, pp. 1479–1492, Apr. 2013.
- [30] D.-K. Woo, J.-H. Choi, M. Ali, and H.-K. Jung, "A novel multimodal optimization algorithm applied to electromagnetic optimization," *IEEE Trans. Magn.*, vol. 47, no. 6, pp. 1667–1673, Jun. 2011.
- [31] K.-Y. Hwang, H. Lin, S.-H. Rhyu, and B.-I. Kwon, "A study on the novel coefficient modeling for a skewed permanent magnet and overhang structure for optimal design of brushless DC motor," *IEEE Trans. Magn.*, vol. 48, no. 5, pp. 1918–1923, May 2012.

- [32] Y.-J. Won et al., "Transfer learning-based design method for cogging torque reduction in PMSM with step-skew considering 3-D leakage flux," *IEEE Trans. Magn.*, vol. 59, no. 11, Nov. 2023, Art. no. 8204905.
- [33] O. Ocak and M. Aydin, "An innovative semi-FEA based, variable magnet-step-skew to minimize cogging torque and torque pulsations in permanent magnet synchronous motors," *IEEE Access*, vol. 8, pp. 210775–210783, 2020.
- [34] M.-M. Koo, J.-Y. Choi, K. Hong, and K. Lee, "Comparative analysis of eddy-current loss in permanent magnet synchronous machine considering PM shape and skew effect using 3-D FEA," *IEEE Trans. Magn.*, vol. 51, no. 11, Nov. 2015, Art. no. 6301104.
- [35] Y. Ichimura, R. Tsunata, M. Takemoto, and J. Imai, "Basic investigation of an IPMSM employing rotor skew for enhancing output power under field weakening control," in *Proc. 50th Annu. Conf. IEEE Ind. Electron.* Soc., 2024, pp. 1–6.
- [36] C. Liu, K. T. Chau, C. H. T. Lee, and Z. Song, "A critical review of advanced electric machines and control strategies for electric vehicles," *Proc. IEEE*, vol. 109, no. 6, pp. 1004–1028, Jun. 2021.
- [37] R. Tsunata, M. Takemoto, S. Ogasawara, and K. Orikawa, "Variable flux memory motor employing double-layer delta-type PM arrangement and large flux barrier for traction applications," *IEEE Trans. Ind. Appl.*, vol. 57, no. 4, pp. 3545–3561, Jul./Aug. 2021.
- [38] R. Jing, G. Wang, G. Zhang, and D. Xu, "Review of field weakening control strategies of permanent magnet synchronous motors," CES Trans. Elect. Machines Syst., vol. 8, no. 3, pp. 319–331, Sep. 2024.
- [39] Y. Hu, S. Zhu, L. Xu, and B. Jiang, "Reduction of torque ripple and rotor eddy current losses by closed slots design in a high-speed PMSM for EHA applications," *IEEE Trans. Magn.*, vol. 58, no. 2, Feb. 2022, Art. no. 8102206.



REN TSUNATA (Member, IEEE) was born in Miyagi Prefecture, Japan, in 1992. He received the B.S., M.S., and Ph.D. degrees in electrical engineering from Hokkaido University, Hokkaido, Japan, in 2015, 2017, and 2021, respectively.

He was with Toyota Motor Corporation, Aichi, Japan, from 2017 to 2018. In 2021, he joined Okayama University, Okayama, Japan, where he was a Research Fellow, and then became an Assistant Professor with the Graduate School of Natural Science and Technology, in 2022, and has been

a Research Associate Professor, since 2023. His research interests include permanent magnet synchronous machines, variable flux motors, and axial flux machines.

Dr. Tsunata is a Member of the Institute of Electrical Engineers of Japan (IEEJ) and The Japan Society of Applied Electromagnetics and Machines (JSAEM). He has been a recipient of four IEEJ Excellent Presentation Awards in 2017, 2020, 2022, and 2023, and the Incentive Award from JSAEM in 2020.



YU ICHIMURA was born in Okayama Prefecture, Japan, in 2000. He received the B.S. and M.S. degrees in electrical engineering from Okayama University, Okayama, Japan, in 2023 and 2025, respectively.

His research interests include electrical machine design and control.



MASATSUGU TAKEMOTO (Member, IEEE) was born in Tokyo, Japan, in 1972. He received the B.S. and M.S. degrees in electrical engineering from the Tokyo University of Science, Noda, Japan, in 1997 and 1999, respectively, and the Ph.D. degree in electrical engineering from the Tokyo Institute of Technology, Tokyo, Japan, in 2005.

In 1999, he joined the Tokyo Institute of Technology as a Research Associate with the Department of Electrical Engineering. In 2004, he joined the Musashi Institute of Technology, Tokyo, Japan,

as a Research Associate with the Department of Mechanical Systems Engineering, where he became a Lecturer in 2005. In 2008, he joined Hokkaido University, Sapporo, Japan, as an Associate Professor with the Graduate School of Information Science and Technology. Since 2020, he has been with Okayama University, Okayama, Japan, where he is a Professor with the Graduate School of Natural Science and Technology. His research interests include permanent magnet synchronous motors, axial gap motors, rare-earthfree motors, bearingless motors, and magnetic bearings.

Dr. Takemoto is a Member of Institute of Electrical Engineers of Japan (IEEJ). He was the recipient of the Nagamori Award from the Nagamori Foundation in 2017, the IEEJ Transaction Paper Award in 2005, the Prize Paper Awards from the Electric Machines Committee of the IEEE Industry Applications Society (IAS) in 2011 and 2019, and the Prize Paper Award from the Electrical Machines Technical Committee of the IEEE Industrial Electronics Society in 2018. He has served as Secretary, Vice-Chair, and Chair of the IEEE IAS Japan chapter in 2008–2009, 2010–2011, and 2012-2013, respectively.



JUN IMAI (Member, IEEE) was born in Okayama prefecture, Japan, in 1964. He received the B.S., M.S., and Ph.D. degrees in electrical engineering from the Department of Electrical Engineering, Kyushu University, Fukuoka, Japan, in 1987, 1989, and 1992, respectively.

He became a Lecturer with Okayama University, Okayama, Japan, in 2000, and has been an Associate Professor, since 2008. His research interests include the modeling and control of distributed parameter systems, especially in performance lim-

itation issues of physical control systems.